Published in IET Renewable Power Generation
Received on 3rd March 2011
Revised on 22nd December 2011
doi: 10.1049/iet-rpg.2011.0052

ISSN 1752-1416

Modelling and control of photovoltaic panels utilising the incremental conductance method for maximum power point tracking

G.J. Kish J.J. Lee P.W. Lehn

Department of Electrical and Computer Engineering, University of Toronto, Toronto, ON, Canada M5S 3G4
E-mail: greg.kish@mail.utoronto.ca

Abstract: For photovoltaic panels, maximum power point tracking (MPPT) is a crucial process to ensure energy capture is maximised. Various tracking algorithms are available for this purpose. Of these, one of the more common presently implemented is the incremental conductance method. However, no linearised small signal model incorporating an incremental conductance-based MPPT process exists. As will be demonstrated, this is attributed to the formation of a degenerate model when conventional linearisation techniques are applied. In this study, a modelling approach is developed that overcomes this deficiency and permits linearisation of the incremental conductance MPPT algorithm. As a case study adopting this developed approach, a complete small signal dynamic model of the incremental conductance method utilising a boost converter is derived. The model is validated against simulations in PSCAD/EMTDC. This study also presents some applications of the model, such as controller design and stability testing. The results demonstrate that the system is highly robust to variations in the lighting condition.

1 Introduction

Sustainable energy development is a key focus in the present-day energy systems research, with the major renewable energy resources being wind, solar and hydro. Of these, solar stands out as having the least environmental footprint. Photovoltaic (PV) panels are currently the prominent means of extracting solar energy. To interface these PV panels with the electrical network, many different connection topologies are available for system designers to utilise [1]. Despite these options, the majority of installations typically integrate a dc–dc converter between the PV panels and grid-connected dc–ac converter. The dc–dc converter ensures that the PV panels are outputting their maximum power and either boosts or bucks the panel voltage to an appropriate level for the dc link, while the dc–ac converter's primary role is to transfer this power to the point of common coupling.

A PV panel converts solar radiation to dc power and possesses a non-linear current–voltage (I–V) output terminal characteristic. This I–V characteristic varies with changes in irradiation level and panel temperature, with the point of maximum output power varying accordingly [2]. In order for the system to work at its optimal power output a control algorithm is required to automatically track the PV panel's maximum power point (MPP). As such, significant research effort has been contributed to devising these MPP tracking (MPPT) algorithms [3–10].

The most common algorithms presently implemented are the hill-climbing (perturb and observe) [7, 9, 11], incremental conductance [6, 12–15] and constant voltage methods [13, 16, 17]. The only advantages of the constant voltage method over the others are its speed and ease of implementation, but these come at a price of reduced energy yield. Both the hill-climbing and the incremental conductance methods may have difficulty finding the MPP when used in large arrays where multiple local maxima occur. However, the hill-climbing method suffers from a slow response time and may also experience difficulty in tracking the MPP if weather conditions change rapidly [18]. Moreover, when compared to incremental conductance, the hill-climbing method may present additional challenges in model synthesis without providing much additional benefit. For instance, the incremental conductance method allows the use of state space control and modelling, which enables the use of established control design tools, stability analysis and rigorous assessment of system robustness to different parameters. For these reasons, the focus of this work pertains to the incremental conductance method, as applied to small and medium power applications (<50 kW).

Recent effort has been put forth towards constructing small signal models of PV systems incorporating different MPPT algorithms [19–23]. A complete representation of the MPPT dynamics, however, is not provided in these publications because of the lack of availability of established dynamic models for the MPPT blocks. The incremental conductance method is one such tracking algorithm without a readily available linearised small signal model. Consequently, existing methods used to characterise dynamics of an incremental conductance-based MPPT

process either give an incomplete picture or have limited use [24–27]. Specifically, in [24, 25] dynamics of the incremental conductance method are evaluated based on logic flowchart representations of the algorithm implemented in MATLAB. These models are relatively complex and do not lend themselves to stability or robustness analyses. In [26] an analytical model of the incremental conductance method was developed to aid in stability analyses. However, the linearisation process assumed a fixed slope to represent the PV panel's non-linear I–V characteristic for operating points near the MPP, and thus the dynamics are not fully captured (as will be shown in section 5). In [27] the incremental conductance method is implemented using a PI compensator that was initially tuned using the Ziegler–Nichols method. Trial and error (heuristic)-based approaches, as opposed to classical control design tools such as frequency-response, are typically employed for controller tuning as the incremental conductance method lacks an established small signal model.

As no linearised small signal models directly addressing the incremental conductance method are readily available in the literature, no systematic procedures exist to (i) calibrate the MPPT controller, (ii) evaluate stability limits or (iii) quantify system robustness.

In order to address these needs a complete linearised small signal dynamic model applicable for the incremental conductance method is derived in this paper. To implement the MPPT algorithm the assumed system topology adopts duty cycle control of a boost converter using a simple PI compensator. A full non-linear model of a PV panel is used as the incremental conductance method inherently relies on the PV panel's slope characteristic. A state-space representation of the system is established to facilitate control design, stability and robustness analyses. The small signal model is validated against a PV system implemented in the PSCAD/EMTDC simulation environment.

2 Incremental conductance method

The operating point for a PV panel which coincides with its maximum power output can be mathematically stated as

$$\frac{I_{\mathrm{pv}}}{V_{\mathrm{pv}}} = -\frac{\mathrm{d}I_{\mathrm{pv}}}{\mathrm{d}V_{\mathrm{pv}}} \tag{1}$$

where I_{pv} and V_{pv} are the PV panel's terminal current and voltage, respectively. In other words, the MPP for a PV panel corresponds to an operating condition where the large signal conductance is equal to the negative of the incremental conductance. To attain maximum power output from a PV panel the incremental conductance method exploits this requirement by utilising a controller to achieve the relationship in (1).

3 Study system

3.1 System topology

A typical PV system interfaces the PV panel and dc–ac converter through a dc–dc converter. For PV panels of small to medium capacity the output voltages are usually lower than the voltage across the dc-link capacitor, thus a boost converter is generally used for the dc–dc stage. As a result, the PV system topology under consideration in this work is presented in Fig. 1.

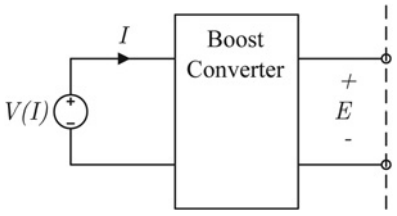

Fig. 1 *PV system configuration for modelling of the incremental conductance method*

The PV panel is represented by a dependent voltage source. The panel voltage, $V(I)$, is assumed to be a function of the panel current, I. The dc-link voltage E is considered to be regulated by a device external to the system (as indicated by the dotted line). This is a fairly reasonable assumption as in most cases the dc-link voltage is either regulated by the dc–ac converter or possibly fixed by a battery energy storage system.

3.2 Controller tracking algorithm

The large signal conductance, $Y(I)$ and incremental conductance, $\tilde{Y}(I)$, are defined with respect to the panel voltage and current

$$Y(I) \triangleq \frac{I}{V(I)} \tag{2}$$

$$\tilde{Y}(I) \triangleq \frac{\mathrm{d}I}{\mathrm{d}V(I)} \tag{3}$$

Similarly, the large signal impedance, $Z(I)$ and incremental impedance, $\tilde{Z}(I)$, are defined

$$Z(I) \triangleq \frac{V(I)}{I} \tag{4}$$

$$\tilde{Z}(I) \triangleq \frac{\mathrm{d}V(I)}{\mathrm{d}I} \tag{5}$$

This implies the following relationships

$$Y(I) = Z(I)^{-1} \tag{6}$$

$$\tilde{Y}(I) = \tilde{Z}(I)^{-1} \tag{7}$$

Relating (2) and (3) by (1) gives the MPPT requirement

$$Y(I) = -\tilde{Y}(I) \tag{8}$$

As it is desired to have a PI compensator force the requirement stated in (8), the error signal input to the compensator, e, is defined

$$e \triangleq -\tilde{Y}(I) - Y(I) \tag{9}$$

4 Modelling challenges

This section outlines the challenges associated with the derivation of a small signal model from a block diagram representation of the physical system using standard linearisation techniques. The discussion also provides the motivation behind choosing the mathematical modelling strategy adopted in Section 5.

doi: 10.1049/iet-rpg.2011.0052

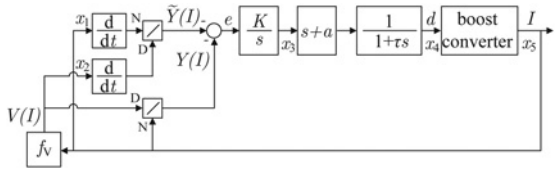

Fig. 2 *Control block diagram for the incremental conductance method*

The incremental conductance term defined by (3) is typically implemented digitally within a micro-controller according to [15]

$$\frac{\mathrm{d}I_k}{\mathrm{d}V_k} = \frac{I_k - I_{(k-1)}}{V_k - V_{(k-1)}} \tag{10}$$

where the voltage and current waveforms are sampled at k (integer) multiples of the sampling period, T_s. However, it must be recognised that (10) is merely a ratio of two differentiators as seen below

$$\frac{\mathrm{d}i(t)}{\mathrm{d}t} \Rightarrow \frac{I_k - I_{(k-1)}}{T_s} \tag{11}$$

$$\frac{\mathrm{d}v(t)}{\mathrm{d}t} \Rightarrow \frac{V_k - V_{(k-1)}}{T_s} \tag{12}$$

where $i(t)$ and $v(t)$ are continuous time current and voltage waveforms, respectively. Based on this observation, continuous time differentiators are used to model the incremental conductance term.

Consider the continuous time control block diagram representation of the incremental conductance method shown in Fig. 2. Here, d is the converter's duty cycle, parameters K and a represent the PI compensator used to drive (9) to zero, and τ is the time constant for a low-pass filter used to remove switching harmonics from the control signals. The f_V block represents the non-linear function which maps I to $V(I)$. The physical implementation of the incremental conductance method dictates the presence of five system states denoted by x_1 through x_5, as indicated in Fig. 2.

With the control system formulated the next step would be to constrain the model to regions near the steady-state operating point (MPP). However, the structure in Fig. 2 leads to a degenerative system that cannot be solved. As will be shown later, this is because of the presence of redundant state variables associated with the MPPT. The redundant state variables, x_1 and x_2 of Fig. 2, stem from the implicit linkage that exists between $Y(I)$ and $\tilde{Y}(I)$, combined with the non-linear function f_V, imposed by the $I-V$ characteristic of the PV panel.

From the preceding discussion it is apparent that another mathematical modelling approach is needed to linearise the system in Fig. 2. To accomplish this, Taylor Series expansions are exploited.

5 System modelling

This section develops detailed modelling of the PV panel and boost converter, based on the initial work in [28]. For clarity, any dependent sources or variables will be explicitly shown as functions of their corresponding independent variable.

5.1 PV panel

The PV panel incorporates the double diode model of the polycrystalline cell in Fig. 3 [29]. The cell is modelled by a photocurrent I_{ph} in parallel with a resistance R_p and two photodiodes, which are represented by the saturation currents I_{s1} and I_{s2}. A resistance R_s is also placed in series with the cell terminal. The cell current, I_c and cell voltage, V_c, are described by the transcendental function [29]

$$I_c = I_{ph} - I_{s1}[\mathrm{e}^{((V_c+I_cR_s)/v_t)} - 1] - I_{s2}\mathrm{e}^{((V_c+I_cR_s)/Av_t)} - \frac{V_c + I_cR_s}{R_p} \tag{13}$$

where

$$v_t = \frac{kT}{e} \tag{14}$$

$$I_{ph} = K_0 S(1 + K_1 T) \tag{15}$$

$$I_{s1} = K_2 T^3 \mathrm{e}^{(K_3/T)} \tag{16}$$

$$I_{s2} = K_4 T^{(1/2)} \mathrm{e}^{(K_5/T)} \tag{17}$$

$$A = K_6 + K_7 T \tag{18}$$

$$R_s = K_8 + \frac{K_9}{S} + K_{10} T \tag{19}$$

$$R_p = K_{11} \mathrm{e}^{(K_{12} T)} \tag{20}$$

Here, T is the PV cell temperature, S is the solar irradiance, k is Boltzmann's constant, e is the electronic charge, v_t is the diode thermal voltage, A is the diode parameter (ideality factor) associated with recombination in the space–charge layer and K_0 through K_{12} are model coefficients.

A combination of N_s series connected cells and N_p parallel cell branches were used to model the PV panel, or in this case an entire PV array. This model neglects any losses associated with cell shading or string mismatching. The parameters used to generate a 35 kW PV array are provided in Appendix 1. The model inputs S and T were assumed as 1000 W/m^2 and 298 K, respectively. The coefficients K_0 to K_{12} used in the empirical relationships (15) through (20) were obtained in [29] from earlier works that reported experimental polycrystalline cell characterisation. Diode parameter A is set to 2 to approximate the Shockley–Read–Hall recombination. Fig. 4 shows the resulting non-linear $I-V$ terminal characteristics for the array. By defining I_0 as the steady-state array current corresponding to the array's maximum power output, $P(I_0)$, the MPP can be characterised with I_0, $V(I_0)$ and $P(I_0)$ of 137.9 A, 253.9 V and 35 kW, respectively.

The 35 kW PV array was implemented in PSCAD/EMTDC as a current controlled voltage source ($V = V(I)$)

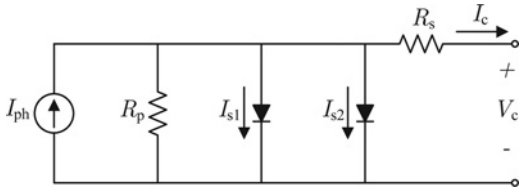

Fig. 3 *Double diode model for the polycrystalline cell*

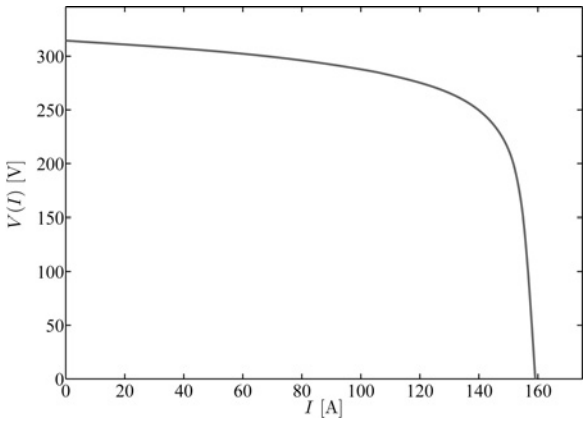

Fig. 4 *PV array non-linear I–V characteristic*

based on the cell model in Fig. 3 and the parameters in Appendix 1.

Fig. 5 provides the $\tilde{Z}(I)$ curve corresponding to the slope of the $I-V$ characteristic in Fig. 4.

5.2 Boost converter

The averaged model for the boost converter is shown in Fig. 6*a* [30]. Forward voltage drops and conductions losses for the diode and switch are neglected. The output load of the converter is represented by the resistor R. The $<>$ brackets denote quantities that are averaged over the switching period. The variable d represents the converter duty cycle.

To obtain a linearised small signal model of Fig. 6*a*, all averaged quantities are replaced by a steady-state dc component (associated with the MPP) and a corresponding small signal variation (e.g. $<I> = I_0 + \Delta I$). After enforcing the previously stated assumption of negligible ΔE, the resulting small signal model for the boost converter is depicted in Fig. 6*b*.

Summing all the voltage drops to zero

$$sL\Delta I = \Delta V(I) - E_0 \Delta d \tag{21}$$

To relate $\Delta V(I)$ and ΔI, a Taylor Series expansion of $V(I)$ is first performed

$$V(I) = V(I_0) + \left.\frac{\partial V(I)}{\partial I}\right|_{I=I_0} \Delta I + \overbrace{H_V(I)}^{\text{higher-order terms}} \tag{22}$$

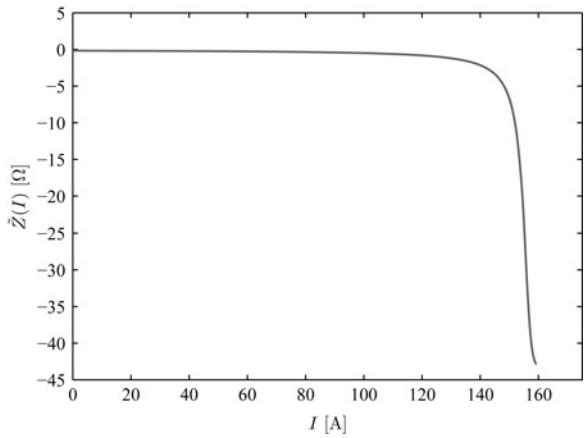

Fig. 5 *PV array incremental impedance*

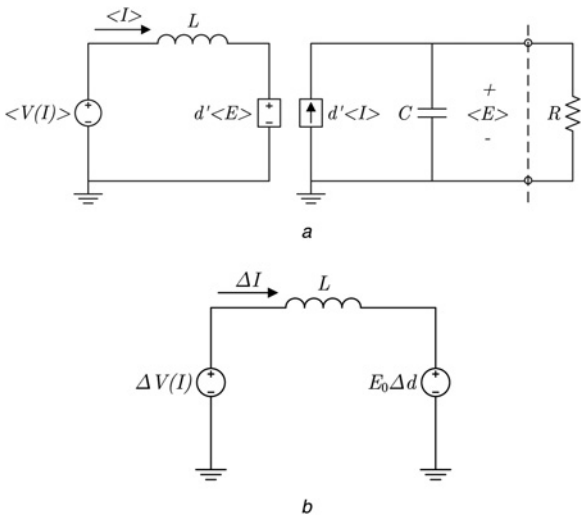

Fig. 6 *Boost converter models*

a Averaged model
b Small signal model

After discarding the steady-state operating point and neglecting all higher-order terms

$$\Delta V(I) \simeq \left.\frac{\partial V(I)}{\partial I}\right|_{I=I_0} \Delta I \tag{23}$$

Noting that the term multiplying ΔI is simply $\tilde{Z}(I_0)$, (23) is substituted into (21) to ascertain the boost converter transfer function

$$\frac{\Delta I}{\Delta d} = \frac{E_0}{sL - \tilde{Z}(I_0)} \tag{24}$$

where $\tilde{Z}(I_0)$ is the incremental impedance at the MPP. Since $\tilde{Z}(I)$ is inherently negative, as illustrated by Fig. 5, the pole of this transfer function will always be in the left half plane.

5.3 Large signal conductance

To determine the relation between $\Delta Y(I)$ and ΔI, a Taylor Series expansion of $Y(I)$ is used

$$Y(I) = Y(I_0) + \left.\frac{\partial Y(I)}{\partial I}\right|_{I=I_0} \Delta I + \overbrace{H_Y(I)}^{\text{higher-order terms}} \tag{25}$$

Substituting (2) into the RHS of (25)

$$Y(I) = Y(I_0) + \left.\frac{\partial (I/(V(I)))}{\partial I}\right|_{I=I_0} \Delta I + \overbrace{H_Y(I)}^{\text{higher-order terms}} \tag{26}$$

After applying the quotient rule to (26) and neglecting all higher-order terms

$$\Delta Y(I) \simeq \left[\frac{V(I_0) - \tilde{Z}(I_0) I_0}{V(I_0)^2}\right] \Delta I \tag{27}$$

By recognising that $\tilde{Z}(I_0) = -V(I_0)/I_0$ at the MPP, (27) is restructured to give the transfer function relating $\Delta Y(I)$

doi: 10.1049/iet-rpg.2011.0052

and ΔI

$$\frac{\Delta Y(I)}{\Delta I} = \frac{2}{V(I_0)} \tag{28}$$

5.4 Incremental conductance

Similar to the approach taken in (25), $\tilde{Y}(I)$ is represented by its Taylor Series expansion

$$\tilde{Y}(I) = \tilde{Y}(I_0) + \left.\frac{\partial \tilde{Y}(I)}{\partial I}\right|_{I=I_0} \Delta I + \overbrace{H_{\tilde{Y}}(I)}^{\text{higher-order terms}} \tag{29}$$

Substituting (7) into the RHS of (29) we obtain

$$\tilde{Y}(I) = \tilde{Y}(I_0) + \left.\frac{\partial (\tilde{Z}(I)^{-1})}{\partial I}\right|_{I=I_0} \Delta I + \overbrace{H_{\tilde{Y}}(I)}^{\text{higher-order terms}} \tag{30}$$

After applying the chain rule to (30) and neglecting all higher-order terms, the transfer function relating ΔI to $\Delta\tilde{Y}(I)$ is determined as

$$\frac{\Delta \tilde{Y}(I)}{\Delta I} = -\frac{1}{\tilde{Z}(I_0)^2}\left.\frac{\mathrm{d}\tilde{Z}(I)}{\mathrm{d}I}\right|_{I=I_0} \tag{31}$$

Note $\mathrm{d}\tilde{Z}(I)/\mathrm{d}I$ is the derivative of the incremental impedance, and is therefore a second-order term. This is contrary to the usual practice employed for small signal modelling where only first-order terms are of interest, and all second-order terms are neglected.

6 System block diagram

Utilising the transfer functions (24), (28) and (31) a complete linearised small signal model of the system is formulated in Fig. 7*a*, where

$$\Upsilon \triangleq \frac{2}{V(I_0)} \tag{32}$$

$$\Phi \triangleq \frac{1}{\tilde{Z}(I_0)^2}\left.\frac{\mathrm{d}\tilde{Z}(I)}{\mathrm{d}I}\right|_{I=I_0} \tag{33}$$

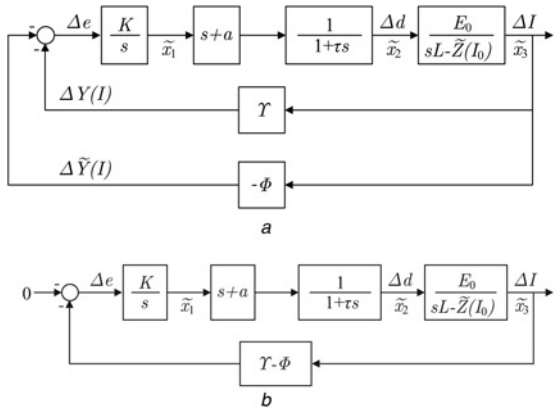

Fig. 7 *Small signal model control block diagrams*

a Complete
b Simplified

A low-pass filter block with time constant τ has been added to filter switching harmonics. A proportional-integral (PI) compensator quantified by K and a is used to control the duty cycle input for the boost converter. The system states are represented by $\tilde{x}_1$, $\tilde{x}_2$ and $\tilde{x}_3$.

To reflect a classical feedback control structure the system block diagram in Fig. 7*a* can be simplified as demonstrated by Fig. 7*b*. It should be stressed here that the feedback term $(\Upsilon - \Phi)\Delta I$ in Fig. 7*b* is neither a direct representation of the conductance $\Delta Y(I)$ nor of the incremental conductance $\Delta\tilde{Y}(I)$ (as provided in Fig. 7*a*), but rather a unique combination of the two.

As discussed earlier, the formulation of a system matrix would enable control design, stability and robustness analyses for the incremental conductance method. Thus, a state-space representation of the system is derived

$$\dot{\tilde{\boldsymbol{x}}} = \begin{bmatrix} 0 & 0 & K(\Phi - \Upsilon) \\ \dfrac{a}{\tau} & \dfrac{-1}{\tau} & \dfrac{K}{\tau}(\Phi - \Upsilon) \\ 0 & \dfrac{E_0}{L} & \dfrac{\tilde{Z}(I_0)}{L} \end{bmatrix} \tilde{\boldsymbol{x}} \tag{34}$$

where

$$\tilde{\boldsymbol{x}} = \begin{bmatrix} \tilde{x}_1 & \tilde{x}_2 & \tilde{x}_3 \end{bmatrix}^{\mathrm{T}} \tag{35}$$

It is important to highlight that the presence of a second-order term within the small signal model is not conventional. Recalling the modelling challenges outlined in Section 4, it becomes clear that the existence of the term $\mathrm{d}\tilde{Z}(I)/\mathrm{d}I$ within the small signal model of Fig. 7*a* enables the elimination of two additional redundant states required for the physical implementation shown in Fig. 2.

7 Model validation

To validate the linearised model of Fig. 7*a*, its output response is compared against simulation results for the complete PV system of Fig. 1 implemented in PSCAD/EMTDC. The PV array is modelled by the non-linear $I-V$ curve in Fig. 4. Bode plot design was used to tune the PI compensator, with $a \simeq -((\tilde{Z}(I_0))/L)$ and K chosen for a phase margin $>60^\circ$. Thus, K and a were selected as 0.26 Ω and 230 s^{-1}, respectively. To ensure controller robustness to parameter variation a sensitivity analysis (see Section 8) should be performed.

To implement (9) in PSCAD/EMTDC, the incremental conductance was determined by sampling the inductor current and voltage waveforms at every switching instance and calculating $(\mathrm{d}I)/\mathrm{d}(V(I))$.

7.1 Simulation results

To investigate the system dynamics, a duty cycle disturbance of 10% was injected for 2 ms. This disturbance temporarily moves the system away from its steady-state operating point and allows the system recovery dynamics to be observed. Fig. 8 provides simulation results showing the response of $V(I)$, I, d, $Y(I)$ and $\tilde{Y}(I)$ to the duty cycle disturbance occurring at $t = 0.1$ s. Once the disturbance is removed, the array voltage and current fully recover to their steady-state (MPP) values after ~20 ms. The small signal model shows excellent agreement with the full PV system implementation in PSCAD/EMTDC, thus validating the model of Fig. 7*a*.

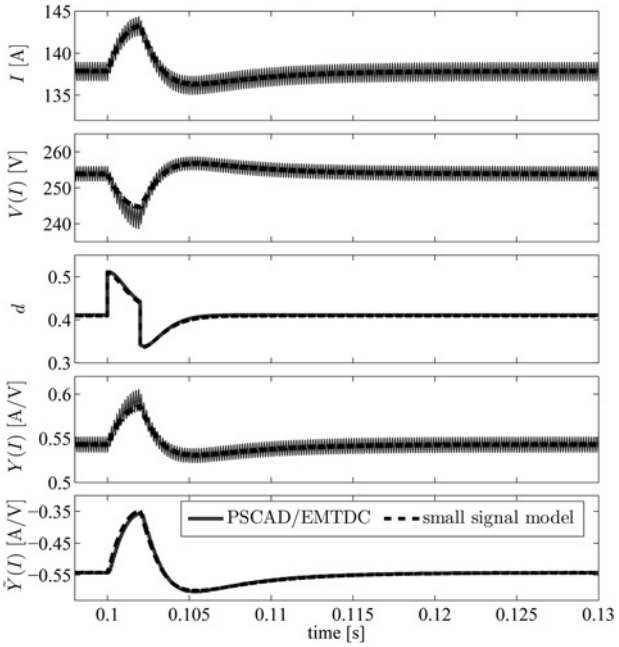

Fig. 8 *Disturbance rejection at $t = 0.1$ s, +10% duty cycle for 2 ms: output response for I, V(I), d, Y(I) and $\tilde{Y}$(I)*

Two additional simulations were performed to observe the PSCAD/EMTDC system dynamics in response to changes in solar irradiance. Figs. 9 and 10 show the response of I, $V(I)$ and d to a step change and ramp change in solar irradiance, respectively. In Fig. 9 a step change in S from 1000 to 875 W/m^2 takes place at $t = 0.15$ s. There is an abrupt drop in array voltage as the step change has essentially introduced a new steady-state MPP, yet the array current cannot change instantaneously because of the boost inductance. The system adapts and properly tracks the new MPP after ~15 ms. In Fig. 10 a ramp change in S from 1000 to 500 W/m^2 is initiated at $t = 0.15$ s, lasting for 500 ms. Even though there is a relatively large and fast change in S, the waveforms transition between the MPPs in a rather controlled manner. These simulation results demonstrate the incremental conductance method is fairly robust to rapidly changing climate conditions.

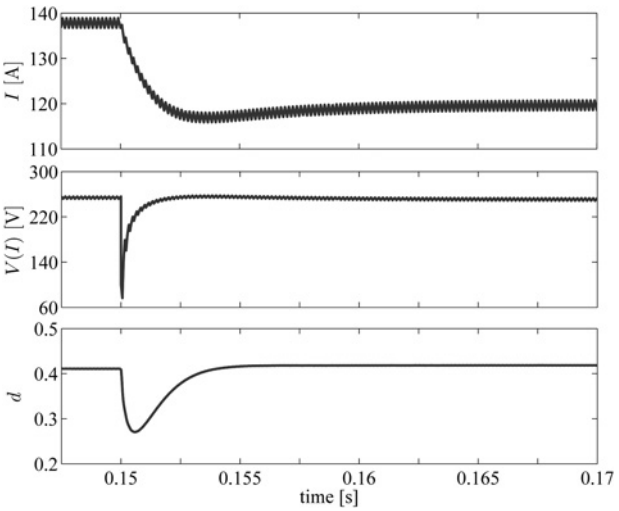

Fig. 9 *Step change in solar irradiance from $S = 1000$ to 875 W/m^2 at $t = 0.15$ s: output response for I, V(I) and d*

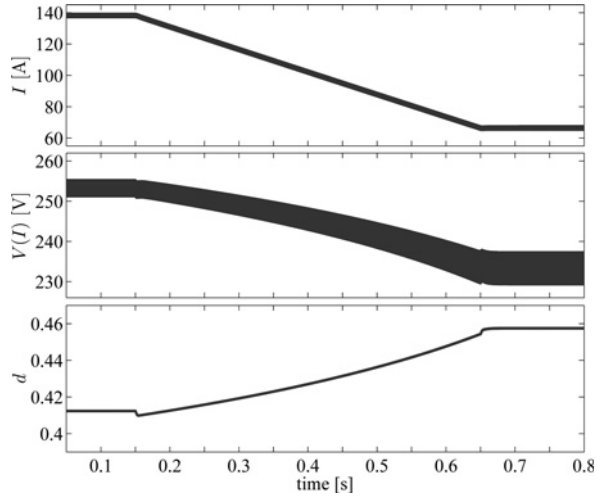

Fig. 10 *Ramp change in solar irradiance from $S = 1000$ to 500 W/m^2, starting at $t = 0.15$ s and ending at $t = 0.65$ s (500 ms ramp duration): output response for I, V(I) and d*

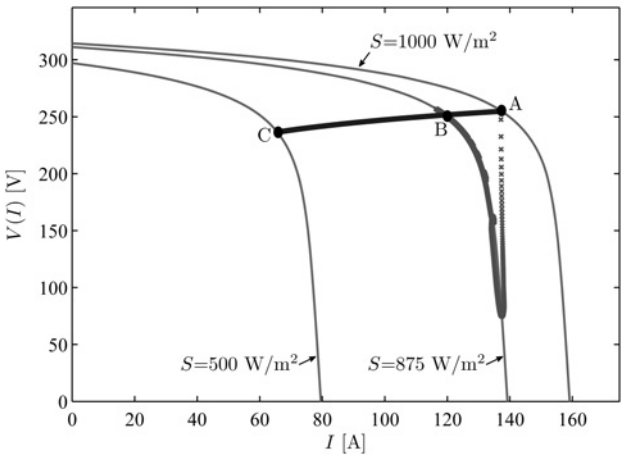

Fig. 11 *PV array I–V curves ($T = 298$ K) with dynamics of I and V(I) superimposed for: (i) step change in solar irradiance from $S = 1000$ to 875 W/m^2 (refer Fig. 9) and (ii) 500 ms duration ramp change in solar irradiance from $S = 1000$ to 500 W/m^2 (refer Fig. 10)*

To illustrate the operating point (MPP) variations of the PV array associated with Figs. 9 and 10, the PV array I–V characteristics for S equal to 1000, 875 and 500 W/m^2 are overlaid in Fig. 11. The MPPs are characterised by points A (137.9 A, 253.9 V), B (119.9 A, 250.4 V) and C (66 A, 235.2 V) for S equal to 1000, 875 and 500 W/m^2, respectively. The dynamics of I and $V(I)$ associated with the step and ramp changes in S are superimposed.

8 Eigenvalue analysis

The system matrix in (34) provides the means to investigate system stability by observing the locus of closed loop poles because of parameter variations or changing steady-state operating points.

For demonstration, an analysis is performed for a system under rated conditions as tabulated in Appendix 2. For a fixed compensator ($K = 0.26\ \Omega$, $a = 230\ \text{s}^{-1}$) the solar irradiance S was varied from 100 to 1000 W/m^2. Fig. 12 shows how the closed loop poles are influenced by the associated MPP variation. As Fig. 12 indicates, small signal

doi: 10.1049/iet-rpg.2011.0052

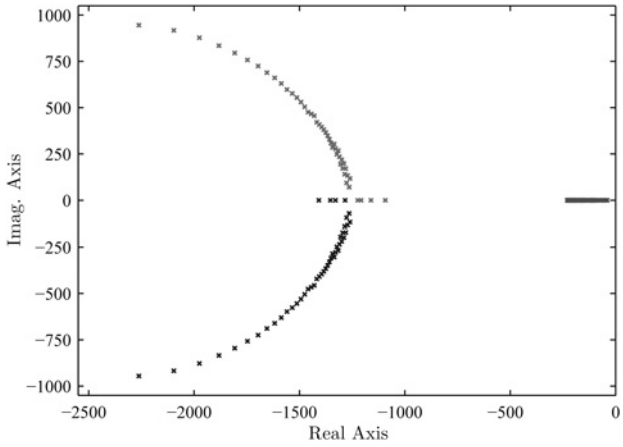

Fig. 12 *Movement of closed loop poles due to changing irradiance: S varied from 100 to 1000 W/m^2 (+20 W/m^2 increments)*

stability is easily determined by observing the locus of eigenvalue locations for the denoted variations in *S*.

9 Conclusion

The incremental conductance method is one of the more common MPPT algorithms presently implemented for small and medium power applications. In this paper a complete linearised small signal model for the incremental conductance MPPT method utilising a boost converter topology has been presented. Owing to the existence of redundant state variables within the control system block diagram, conventional linearisation techniques initially led to an unsolvable system. To overcome this challenge an alternative modelling approach employing Taylor Series expansions was adopted. The model's output response shows very good agreement with simulation results of a PV system implemented in PSCAD/EMTDC. The derivation of a state-space representation for the system permits control design, stability and robustness analyses. It has been demonstrated that the incremental conductance MPPT algorithm is highly robust to variations in the solar irradiance. Based on the presented modelling technique, PV solar arrays with incremental conductance-based MPPT can now be entirely integrated into eigenvalue analysis software tools alongside conventional generators. The modelling approach developed here can be readily adapted to PV system configurations incorporating different converter topologies.

10 References

1 Kjaer, S.B., Pedersen, J.K., Blaabjerg, F.: 'A review of single-phase grid-connected inverters for photovoltaic modules', *IEEE Trans. Ind. Appl.*, 2005, **41**, (5), pp. 1292–1306

2 Xiao, W., Dunford, W.G.: 'Evaluating maximum power point tracking performance by using artificial lights'. Proc. Conf. on IEEE Industrial Electronics Society (IECON), Vancouver, British Columbia, November 2004, pp. 2883–2887

3 Masoum, M.A.S., Dehbonei, H., Fuchs, E.F.: 'Theoretical and experimental analyses of photovoltaic systems with voltage and current-based maximum power-point tracking', *IEEE Trans. Energy Convers.*, 2002, **17**, (4), pp. 514–522

4 Jain, S., Agarwal, V.: 'Comparison of the performance of maximum power point tracking schemes applied to single-stage grid-connected photovoltaic systems', *IET Electr. Power Appl.*, 2007, **1**, (5), pp. 753–762

5 Liang, T.J., Kuo, Y.C., Chen, J.F.: 'Single-stage photovoltaic energy conversion system', *IEE Proc. Electr. Power Appl.*, 2001, **148**, (4), pp. 339–344

6 Yusof, Y., Sayuti, Y.S.H., Latif, M.A., Wanik, M.Z.C.: 'Modeling and simulation of maximum power point tracker for photovoltaic system'. Proc. National Power and Energy Conf. (PECon), Kuala Lumpur, Malaysia, November 2004, pp. 88–93

7 Femia, N., Petrone, G., Spagnuolo, G., Vitelli, M.: 'Optimization of perturb and observe maximum power point tracking method', *IEEE Trans. Power Electron.*, 2005, **20**, (4), pp. 963–973

8 Patel, H., Agarwal, V.: 'Maximum power point tracking scheme for PV systems operating under partially shaded conditions', *IEEE Trans. Ind. Electron.*, 2008, **55**, (4), pp. 1689–1698

9 Piegari, L., Rizzo, R.: 'Adaptive perturb and observe algorithm for photovoltaic maximum power point tracking', *IET Renew. Power Gener.*, 2010, **4**, (4), pp. 317–328

10 Esram, T., Chapman, P.L.: 'Comparison of photovoltaic array maximum power point tracking techniques', *IEEE Trans. Energy Convers.*, 2007, **22**, (2), pp. 439–449

11 Fermia, N., Granozio, D., Petrone, G., Vitelli, M.: 'Predictive adaptive MPPT perturb and observe method', *IEEE Trans. Aerosp. Electron. Syst.*, 2007, **43**, (3), pp. 934–950

12 Roman, E., Alonso, R., Ibanez, P., Elorduizapatarietxe, S., Goitia, D.: 'Intelligent PV module for grid-connected PV systems', *IEEE Trans. Ind. Electron.*, 2006, **53**, (4), pp. 1066–1073

13 Elgendy, M.A., Zahawi, B., Atkinson, D.J.: 'Analysis of the performance of DC photovoltaic pumping systems with maximum power point tracking'. Proc. IET Conf. on Power Electronics, Machines and Drives (PEMD), York, UK, April 2008, pp. 426–430

14 Safari, A., Mekhilef, S.: 'Simulation and hardware implementation of incremental conductance MPPT with direct control method using cuk converter', *IEEE Trans. Ind. Electron.*, 2011, **58**, (4), pp. 1154–1161

15 Liu, F., Duan, S., Liu, F., Liu, B., Kang, Y.: 'A variable step size INC MPPT method for PV systems', *IEEE Trans. Ind. Electron.*, 2008, **55**, (7), pp. 2622–2628

16 Kawamura, T., Harada, K., Ishihara, Y., *et al.*: 'Analysis of MPPT characteristics in photovoltaic power system', *Sol. Energy Mater. Sol. Cells*, 1997, **47**, (1–4), pp. 155–165

17 Kobayashi, K., Matsuo, H., Sekine, Y.: 'An excellent operating point tracker of the solar-cell power supply system', *IEEE Trans. Ind. Electron.*, 2006, **53**, (2), pp. 495–499

18 Hussein, K.H., Muta, I., Hoshino, T., Osakada, M.: 'Maximum photovoltaic power tracking: an algorithm for rapidly changing atmospheric conditions', *IEE Proc. Gener. Transm. Distrib.*, 1995, **142**, (1), pp. 59–64

19 Villalva, M.G., de Siqueira, T.G., Ruppert, E.: 'Voltage regulation of photovoltaic arrays: small-signal analysis and control design', *IET Power Electron.*, 2010, **3**, (6), pp. 869–880

20 Figueres, E., Garcera, G., Sandia, J., Gonzalez-Espin, F., Rubio, J.C.: 'Sensitivity study of the dynamics of three-phase photovoltaic inverters with an LCL grid filter', *IEEE Trans. Ind. Electron.*, 2009, **56**, (3), pp. 706–717

21 Femia, N., Lisi, G., Petrone, G., Spagnuolo, G., Vitelli, M.: 'Distributed maximum power point tracking of photovoltaic arrays: novel approach and system analysis', *IEEE Trans. Ind. Electron.*, 2008, **55**, (7), pp. 2610–2621

22 Venturini, R.P., Scarpa, V.V.R., Spiazzi, G., Buso, S.: 'Analysis of limit cycle oscillations in maximum power point tracking algorithms'. Proc. IEEE Power Electronics Specialists Conf. (PESC), Rhodes, Greece, June 2008, pp. 378–384

23 Villalva, M.G., Espindola, M.F., Siqueira, T.G., Ruppert, E.: 'Modeling and control of a three-phase isolated grid-connected converter for photovoltaic applications', *Controle Autom. Soc. Bras. Autom.*, 2011, **22**, (3), pp. 215–228

24 Azevedo, G.M.S., Cavalcanti, M.C., Oliveira, K.C., Neves, F.A.S., Lins, Z.D.: 'Comparative evaluation of maximum power point tracking methods for photovoltaic systems', *ASME J. Sol. Energy Eng.*, 2009, **131**, (3), pp. 1–8

25 Zegaoui, A., Aillerie, M., Petit, P., Sawicki, J.P., Charles, J.P., Belarbi, A.W.: 'Dynamic behaviour of PV generator trackers under irradiation and temperature changes', *Sol. Energy*, 2011, **85**, (11), pp. 2953–2964

26 Ahmed, E.M., Shoyama, M.: 'Stability study of variable step size incremental conductance/impedance MPPT for PV systems'. Proc. IEEE Int. Conf. on Power Electronics and ECCE Asia (ICPE ECCE) Jeju, Republic of Korea, 30 May–3 June 2011, pp. 386–392

27 Nafeh, A.E.-S.A.: 'A modified MPPT control loop for PV/battery-charging system using PI controller optimally tuned with GA', *Int. J. Numer. Model., Electron. Netw. Devices Fields*, 2011, **24**, (2), pp. 111–122

28 Lee, J.J.: 'Modeling and control of photovoltaic panels utilizing the incremental conductance method for maximum power point tracking'. M. Eng. report, Electrical and Computer Engineering, University of Toronto, 2009
29 Chowdhury, S., Chowdhury, S.P., Crossley, P.: 'Microgrids and active distribution networks' (Institution of Engineering and Technology, 2009)
30 Erickson, R.W., Maksimović, D.: 'Fundamentals of power electronics' (Springer, 2001, 2nd edn.)

11 Appendix 1: data for double diode model of the polycrystalline cell

The double diode polycrystalline cell model data used to generate the $I-V$ characteristic curve for the 35 kW PV array is summarised in Table 1. This numerical data was taken directly from [29], which utilised the data to facilitate various MPP tracking case studies on a similar PV system. To account for parasitics a lumped panel capacitance of 30 nF/kW was assumed for the PV array.

Table 1 Polycrystalline cell double diode model data

Parameter	Value
no. of parallel cells, N_p	8760
no. of series cells, N_s	720
solar irradiance, S (W/m^2)	1000
PV cell temperature, T (K)	298
Boltzmann's constant, k (J/K)	1.3806×10^{-23}
electronic charge, e (C)	1.6022×10^{-19}
coefficient, K_0	-5.729×10^{-7}
coefficient, K_1	-0.1098
coefficient, K_2	44.5355
coefficient, K_3	-1.264×10^{4}
coefficient, K_4	11.8003
coefficient, K_5	-7.3174×10^{3}
coefficient, K_6	2
coefficient, K_7	0
coefficient, K_8	1.47
coefficient, K_9	1.6126×10^{-3}
coefficient, K_{10}	-4.47×10^{-3}
coefficient, K_{11}	2.3034×10^{6}
coefficient, K_{12}	-2.8122×10^{-2}

12 Appendix 2: system data

The system data used for the small signal model validation are summarised in Table 2.

Table 2 System data ($S = 1000$ W/m^2, $T = 298$ K)

Parameter	Value
$P(I_0)$ (kW)	35
I_0 (A)	137.9
$V(I_0)$ (V)	253.9
$Y(I_0)$ (A/V)	0.543
$\tilde{Y}(I_0)$ (A/V)	-0.543
$\tilde{Z}(I_0)$ (Ω)	-1.84
$\left.\frac{d\tilde{Z}(I)}{dI}\right\|_{I=I_0}$ (Ω/A)	-0.123
E_0 (V)	430
L (mH)	8
K (Ω)	0.26
a (s^{-1})	230
τ (ms)	0.4
f_{sw} (kHz)	6

doi: 10.1049/iet-rpg.2011.0052